Rydberg crystallization detection by statistical means

D. Breyel,[1] T. L. Schmidt,[2,3] and A. Komnik[1]

[1]*Institut für Theoretische Physik, Universität Heidelberg, Philosophenweg 19, D-69120 Heidelberg, Germany*

[2]*Department of Physics, Yale University, 217 Prospect Street, New Haven, Connecticut 06520, USA*

[3]*Departement Physik, Universität Basel, Klingelbergstrasse 82, CH-4056 Basel, Switzerland*

(Received 19 March 2012; published 3 August 2012)

We investigate an ensemble of atoms which can be excited into a Rydberg state. Using a disordered quantum Ising model, we perform a numerical simulation of the experimental procedure and calculate the probability distribution function $P(M)$ to create a certain number of Rydberg atoms M, as well as their pair-correlation function. Using the latter, we identify the critical interaction strength above which the system undergoes a phase transition to a Rydberg crystal. We then show that this phase transition can be detected using $P(M)$ alone.

DOI: 10.1103/PhysRevA.86.023405 PACS number(s): 32.80.Rm, 75.10.Pq, 64.70.Tg, 34.20.Cf

I. INTRODUCTION

Recent experimental progress in producing and controlling highly excited atomic and molecular aggregates has triggered a number of experimental and theoretical works on interacting Rydberg systems [1–16]. One of the most prominent phenomena observable in such systems is the dipole blockade [17,18], which is a consequence of effective interactions between atoms in Rydberg states with principal quantum numbers, $n \sim 30$–80 [19]. The physical reason for the blockade can be summarized as follows: the large dipole moment of a Rydberg atom induces sizable energy-level shifts in the atoms in its vicinity. As a result, atoms within a certain blockade radius R_B cannot be excited, even though they are subjected to the same electromagnetic field as the proper Rydberg atoms.

Typical experiments are conducted on atom ensembles at ultralow temperatures and probe these systems on time scales during which almost no particle movement is possible. Therefore, the cloud of atoms can be considered as "frozen" in a more or less disordered constellation [20]. After the required fine-tuned electromagnetic fields are switched on, a number of atoms undergo a transition into the highly excited Rydberg states. If R_B is larger than the average interatomic distance, then only a fraction of the atoms can be excited, while the rest remain in the ground state due to the blockade effect.

The spatial arrangement of the Rydberg atoms within the cloud has very interesting features. In Refs. [21,22], the concept of a Rydberg crystal was put forward. The blockade region formed around an excited atom can be modeled as an effective repulsive interaction between the Rydberg atoms. It might be responsible for an emergent long-range order of the Wigner crystal type [22,23]. However, its detection is extremely difficult. The primary method for detecting long-range order is spectroscopy, which is difficult to reliably realize in experiments [24]. Other experiments benefit from the low ionization energy of the Rydberg atoms by (pulsed) electric-field ionization (cf. Refs. [7,11,13,14,17,19,20,25–39]).

In this paper, we propose a statistical method of detecting and analyzing the physical properties of the Rydberg crystallization phenomenon and discuss its predictive power. The idea originates in the experimental procedure itself. A typical measurement cycle starts with the generation of an ultracold atomic cloud and the subsequent excitation of a fraction of the atoms to a Rydberg state. Afterwards, measurements are performed, during which the Rydberg atoms are eventually deexcited. Then, the system is ready for another preparation [31,33,39–41]. An important point is that the experiments are performed with the same number of atoms and using the same electromagnetic fields in every cycle. However, since the arrangement of atoms varies between cycles, it is necessary to calculate statistical averages of the observables of interest. The simplest observable is the number of Rydberg atoms M in the cloud. The fact that, for a given M, a regular arrangement of the Rydberg atoms on a lattice minimizes their interaction energy, should be visible in the probability distribution $P(M)$. As we shall show below, there are indeed differences between the histograms for crystallized and random phases. However, the pair-correlation function turns out to possess even higher predictive power [37,42].

This paper is organized as follows. In Sec. II, we shall introduce the model and connect its parameters to possible experimental setups. We shall define the relevant observables and explain the details of our numerical implementation. The results of the calculation together with a thorough analysis of the arising features is contained in Sec. III. Section IV is devoted to the summary of results.

II. THE MODEL AND SIMULATION METHOD

We assume that in every measurement cycle the system consists of N atoms located at randomly chosen positions, $\mathbf{r}_i, i = 1, \ldots, N$, uniformly distributed over the entire system volume [43]. We focus on the case of a frozen Rydberg gas, where the kinetic energy is negligible. Each of the atoms can either be excited to a Rydberg state or stay in its ground state. Since the electrostatic properties do not depend on the details of the Rydberg states, each atom can be modeled as a two-level system, and we describe the ensemble as a set of N randomly arranged, interacting spin-1/2 systems. Hence, the Hamiltonian reads [22,44]

$$H = -\frac{\Delta}{2}\sum_{i=1}^{N}\sigma_z^{(i)} + \frac{\Omega}{2}\sum_{i=1}^{N}\sigma_x^{(i)} + C\sum_{i=2}^{N}\sum_{j=1}^{i-1}\frac{\left(1+\sigma_z^{(i)}\right)\left(1+\sigma_z^{(j)}\right)}{|\mathbf{r}_i - \mathbf{r}_j|^6}, \quad (1)$$

where $\sigma_{x,z}^{(i)}$ denote the Pauli matrices and index i enumerates the atoms of the ultracold cloud. This can be interpreted as a generalized spin-1/2 quantum Ising model. Ω is the frequency of the exciting laser and, in the spin language, represents a magnetic field perpendicular to the quantization axis, which we chose to be the z axis. The detuning, i.e., the difference between the laser frequency to the resonance frequency of the Rydberg state, is denoted by Δ. It corresponds to a magnetic field applied in the z direction. The third parameter, C, indicates the strength of an effective interaction between excited atoms and causes the dipole blockade explained above [45]. The case $\Delta = 0$ has been intensively studied in Ref. [22], where a possibility for a quantum phase transition was pointed out. We would like to concentrate on the case $\Delta > 0$ because otherwise it is energetically not favorable to excite atoms. That is why we use Δ as our energy unit, which we use in all subsequent plots and equations.

An adequate modeling of the system also requires geometrical constraints describing the trap potentials. In the following, we shall consider different scenarios: (i) a one-dimensional (1D) system with open boundaries [46], (ii) a 3D system with open boundaries, and (iii) a 1D system with periodic boundary conditions. Options (i) and (ii) are very natural models for realistic experiments, but make it difficult to extrapolate the presented numerical results towards realistic system sizes. Option (iii), on the other hand, is perfectly suitable for the calculation of correlation functions and is easily scalable to large system lengths. The crucial feature of our 1D model is a rather large "coordination number," i.e., the number of atoms which interact significantly with any given Rydberg atom. This feature is shared by any generic 3D realization of the system up to some irrelevant spatial distribution parameter. That is why we believe that the physics in 3D is expected to be very similar to our 1D model.

Just as in the actual experiments, we calculate averages over the large number of different, randomly sampled atom arrangements. In every cycle, the effective model is a long-range quantum Ising model with a set of coupling constants generated by the atom positions $\mathbf{r}_i$. For every such constellation, we determine the ground state and evaluate the number of Rydberg atoms M (which is equivalent to the magnetization in the Ising model), the density profile, and correlation functions. In most experiments, the Rydberg systems are not expected to be in the ground state. However, as was shown in Refs. [47,48] with the help of chirped laser pulses, any given system can safely be prepared in its ground state. The most difficult task in theory is finding the ground state. We use one method, namely, numerical diagonalization of the Hamiltonian matrix, in three different variations. For small atom numbers (up to $N \approx 12$), the Hamiltonian can be diagonalized exactly. For larger numbers of atoms ($N \approx 30$), we truncate the Hilbert space in different ways in order to speed up the numerical diagonalization. On the one hand, this truncation can be done by only keeping states in which the number of Rydberg atoms M remains below a certain threshold M^*. A different approach is to only use the basis states with the lowest energy expectation values to create an effective Hamiltonian, which is then diagonalized. We checked the reliability of both procedures by changing the respective cutoff parameter.

In contrast to the case $\Omega = 0$ considered in Ref. [49], this method is able to capture the physical effects caused by finite Ω. Still, especially in the case of larger numbers of atoms, our method is approximative in Ω and is most reliable for small values of Ω/Δ. In some special parameter configurations, the ground state can be obtained analytically (for an effective model) and a phase transition is predicted for high [50] and low densities of atoms [51,52].

To calculate the number of Rydberg atoms and the correlation function, which is also analyzed by Monte Carlo simulations in Ref. [16], we proceed as follows. For a given random distribution of atoms, the Hamiltonian matrix is expressed in a basis consisting of states in which an integer number of atoms is in the Rydberg state, while the rest are in the ground state. The corresponding Hilbert space is then truncated as explained above, and the smallest eigenvalue and the corresponding eigenvector (the ground state $|\mathrm{GS}\rangle$) are obtained numerically. The number of Rydberg atoms in the ground state is now found from

$$M = \frac{1}{2}\sum_{i=0}^{\tilde{N}} M(i)|v_i|^2, \tag{2}$$

where $\tilde{N}$ is the dimension of the truncated Hilbert space, $M(i) = \sum_{j=1}^{N}\langle i|(1+\sigma_z^{(j)})|i\rangle$ is the number of Rydberg atoms in the basis state $|i\rangle$, and $v_i = \langle i|\mathrm{GS}\rangle$ is the overlap between $|i\rangle$ and the ground state. One easy way of numbering the basis states is to assign a "1" to a Rydberg atom and a "0" to a ground-state atom. In this way, every basis state can be uniquely mapped to the binary representation of a number $i \in \mathbb{N}_0$. The resulting M are then plotted as a histogram for the (usually quite large) number of ultracold atom cloud realizations.

At this point, we would like to note that there is a second method of producing the histogram of the number of Rydberg atoms. Instead of taking the quantum mechanical expectation value of the number of Rydberg atoms of the ground state of a certain arrangement of atoms, we can project on the subspaces that belong to a definite number of Rydberg atoms. That gives a histogram of probabilities for every single arrangement of atoms, which then can be summed to give an overall histogram. This technique might seem to be even closer to the experimental realization than the procedure presented above since it includes a measurement which is represented by the projection operator. The results of both methods qualitatively agree with each other, therefore we chose to show those of the former method only. Furthermore, we calculate the pair-correlation function

$$g(\mathbf{r}) = \langle \rho_{\mathrm{Rydberg}}(\mathbf{r})\rho_{\mathrm{Rydberg}}(0)\rangle, \tag{3}$$

where $\rho_{\mathrm{Rydberg}}(\mathbf{r})d\mathbf{r}$ denotes the number of Rydberg atoms in a volume element $d\mathbf{r}$ around the point $\mathbf{r}$. The first step is to divide the interval of possible distances between two atoms ($[0; L/2]$ for periodic boundary conditions) into k subintervals of equal length. Calculating the ground state $|\mathrm{GS}\rangle$ for a given distribution of atoms yields the coefficients v_i. In the next step, we consider a single pair of atoms and measure their distance in the current distribution of atoms. This distance lies within one of the aforementioned subintervals. To the value which is already stored for this subinterval, we now add the sum of all

$|v_i|^2$ that correspond to a basis state in which both of the atoms of the considered pair are in the Rydberg state. After repeating this procedure for every possible pair of atoms, we start over by generating a new random distribution. The cumulative sum of all samples treated in this way then gives the total correlation function for a given set of parameters.

III. RESULTS AND DISCUSSION

Let us first discuss the simplest case of a noninteracting system, $C = 0$. In this case, the problem is exactly solvable and the number of Rydberg atoms is given by

$$M_0 = \frac{N}{2}\left(1 + \frac{1}{\sqrt{1+\Omega^2/\Delta^2}}\right). \tag{4}$$

In the noninteracting limit, this value is independent of the positions $\mathbf{r}_i$ of the atoms. Therefore, the histogram $P(M)$ becomes trivial, $P(M) = \delta(M - M_0)$. The density distribution $\rho_0 = \langle \rho_{\text{Rydberg}}(\mathbf{r}) \rangle$, averaged over many realizations, is uniform, and the pair-correlation function $g(\mathbf{r}) = \rho_0^2$ is constant.

The situation changes drastically for any nonzero C. Figure 1 shows the data for the density distribution $\langle \rho_{\text{Rydberg}}(\mathbf{r}) \rangle$ in 1D and 3D systems with open boundaries. While for weak interactions the Rydberg atoms tend to populate the boundaries, in the case of strong interactions, a sizable fraction of the atoms is redistributed towards the system's bulk, indicating that long-range order is established in the system. As we are dealing with a system with long-range interactions, the numerical complexity is determined by the number of Rydberg atoms and not by the precise geometry of the system. On the other hand, going to higher dimensions at fixed atom number N increases the surface/bulk ratio and thus makes the detection of long-range order more cumbersome. Therefore, we shall concentrate on quasi-1D systems from now on. Nonetheless, we have conducted a number of simulations on 3D systems and found comparable results; see, e.g., Fig. 1 for the density profile of a 3D system. We also would like to remark that an experimentally realizable cigar-shaped confining potential

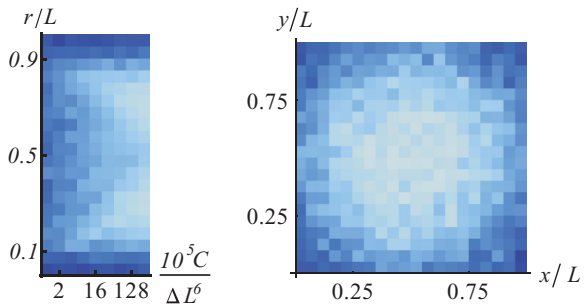

FIG. 1. (Color online) Density distribution of Rydberg atoms; darker color indicates higher density. Left panel: 1D density as a function of interaction strength. The system boundaries are preferred. Strong interactions produce a single peak in the center. Parameters: $\Omega/\Delta = 0.1$ and $N = M^* = 6$ atoms (no cutoff, exact diagonalization). Right panel: 2D projection of a 3D system with $N = M^* = 6, \Omega/\Delta = 4$, and $C = 10$ in a cube with open boundaries. There is a low density at the center of the volume, while it is high in the corners.

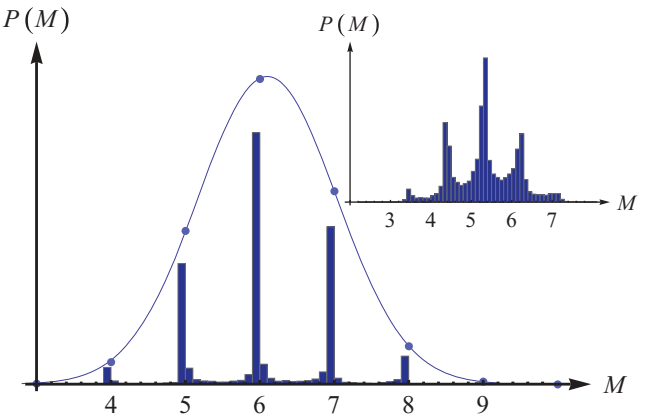

FIG. 2. (Color online) Histogram of the number of Rydberg atoms with Gaussian fit. The data points shown are the cumulative sum of all bins in the interval $[n - 0.5, n + 0.5]$. The features of the plot are explained in the text. Parameters: $\Omega/\Delta = 0.1, C/(\Delta L^6) = 4 \times 10^{-7}$, with $N = 10 = M^*$ atoms (which corresponds to no cutoff). Inset: Histogram for $\Omega/\Delta = 0.64, C/(\Delta L^6) = 5 \times 10^{-7}$, with $N = 10 = M^*$ atoms.

(with a typical radius smaller than R_B) can very well be approximated by the quasi-1D geometry considered here.

Figure 2 shows a typical result for the histogram $P(M)$. For $\Omega = 0$, the number of Rydberg atoms commutes with the Hamiltonian, so the ground state for a given set of position $\{\mathbf{r}_i\}$ has an integer expectation value M of Rydberg atoms. The distribution $P(M)$, generated by considering all arrangements $\{\mathbf{r}_i\}$, thus becomes a series of discrete, weighted peaks at integer values M. For small $0 < \Omega \ll \Delta$, these peaks broaden up, but the distribution remains more or less discrete. Increasing Ω leads to further broadening until eventually a continuous distribution is approached; see inset of Fig. 2.

Surprisingly, in most cases the envelope of the histogram can fairly well be fitted by a Gaussian, as opposed to the Poissonian used, e.g., in Ref. [30]. Nonetheless, the distribution function's higher-order cumulants are not exactly zero and depend on C, which indicates a slight deviation from the Gaussian distribution. The mean μ and the variance σ for a series of simulations are plotted in Fig. 3. Very interestingly, the $\mu(C)$ dependence is given by a power law with an exponent, which changes abruptly from ≈ -0.05 to ≈ -0.1 at around $C/(\Delta L^6) \approx 10^{-6}$, where L is the system length. We find this change to be a harbinger of a phase transition in the system. Both the mean and the width of the distribution function decrease as a function of C because a stronger repulsion

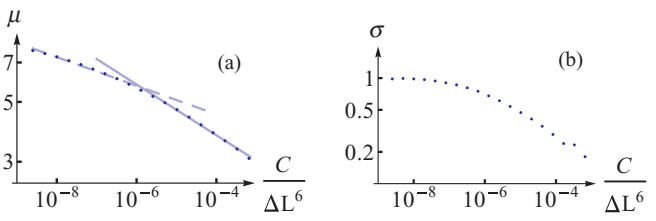

FIG. 3. (Color online) Average number of (a) Rydberg atoms μ and (b) variance σ in dependence on C (double-log plots). The straight lines in (a) are guides for the eye only. The parameters for all plots are $\Omega/\Delta = 0.2$ with $N = 10 = M^*$ atoms.

increases the blockade radius R_B. This qualitative behavior is independent of the value of Ω. If one plots the mean and the variance as functions of Ω, then the general behavior of the mean $\mu(\Omega)$ is qualitatively the same as for the noninteracting case [$\mu(\Omega) = \mu(\Omega, C = 0)$; cf. Eq. (4)] for $\Omega < \Omega^*$, where $\Omega^* = \max(C/L^6, \Delta)$ is the largest energy scale in the system. For $\Omega > \Omega^*$, the spin-flip term dominates the Hamiltonian (1) and M tends to $N/2$. The only effect of C is the change in the overall amplitude of the curve.

In addition to the mean and variance shown in Fig. 3, we analyzed the Mandel Q parameter, which is defined as [53]

$$Q = \frac{\langle M^2 \rangle - \langle M \rangle^2}{\langle M \rangle} - 1. \tag{5}$$

Being in the range $[-0.85, -0.95]$, its behavior is in good agreement with the sub-Poissonian values predicted in Refs. [54,55]. As was realized in Ref. [30], this points towards an efficient Rydberg blockade.

Another interesting quantity is the pair-correlation function $g(r)$, which is defined as the probability of finding a Rydberg atom at a distance r from another Rydberg atom. In order to exclude boundary effects, we now switch to periodic boundary conditions. To be able to handle computations with larger numbers of atoms, we change the truncation procedure to one in which we consider only a fixed number of basis states. This enables us to approach $N \approx 30$. This set of states is chosen to be the one with the smallest diagonal elements in the Hamiltonian matrix. We thoroughly investigated the effect of the truncation by considering the same system with different numbers of contributing states. We find that the result is almost independent of the number of states, as long as it exceeds a certain threshold. All plots displayed in this paper meet this requirement.

A typical correlation function is shown in Fig. 4 and is qualitatively comparable to the ones shown in Refs. [16,56], which are computed within a different model and for a time-evolved state, respectively. On the right panel, one can see additional smaller peaks, which originate from the periodic boundary conditions, on the left side of two principal peaks. This feature, which is known as aliasing, arises in the following way: in the plots shown in Fig. 4 (and in any other plot of a correlation function in this work), our physically meaningful

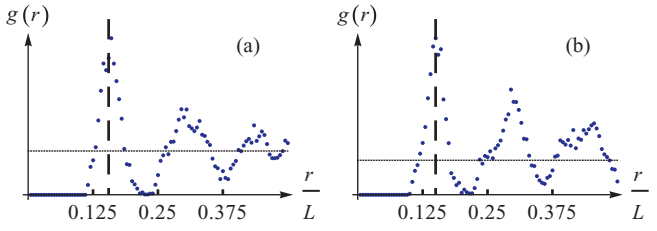

FIG. 4. (Color online) (a) Correlation function with adjustment of the system length in such a way that main and secondary peaks coincide, $C/(\Delta L^6) = 7.5 \times 10^{-6}$. (b) Correlation function as a function of distance. The aliasing can be seen in the shoulders of the second and third maximum, $C/(\Delta L^6) = 4 \times 10^{-6}$. For both correlation functions, $N = 30$ and $\Omega/\Delta = 25$. The dashed vertical line indicates where to read off the blockade radius (used in later plots).

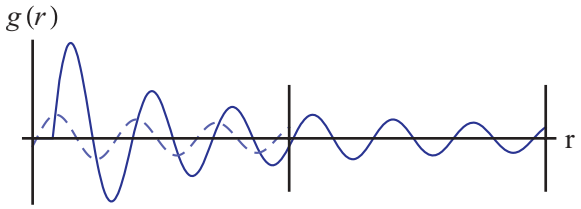

FIG. 5. (Color online) Schematic illustration of the effect shown in Fig. 4. The dashed line is part of the correlation function in the right interval shifted by the length of the interval. The sum of the dashed and solid curve in the left interval is a curve with main peaks that have secondary peaks on their shoulders. The secondary peak on the shoulder of the first peak is suppressed because of the blockade phenomenon.

domain of definition is the interval $[0, L/2]$ since $L/2$ is the maximum distance between two atoms in a 1D system with periodic boundary conditions. In principle, one could extrapolate this correlation function to larger distances. Since we are not able to resolve those, the correlation function is mapped onto the given interval periodically. So the additional peaks appearing here are basically the fifth- and sixth-order peaks of the correlation function. Figure 5 illustrates this behavior, which is also known from the numerical realization of Fourier transforms with finite frequency cutoff [57]. This effect can be hidden when one uses such parameter values at which L and R_B are commensurate; see the left panel of Fig. 4. Using this control prescription, we have calculated $g(r)$ for a very large number of samples for a number of different interaction strengths.

As expected, one can immediately identify the blockade radius R_B as the position of the first maximum. It is the distance between two atoms up to which it is disadvantageous to excite both of them to the Rydberg state. Obviously, it is nonzero for all interaction strengths C. The actual $R_B(C)$ dependence is very interesting and is plotted in Fig. 6. Very naturally, R_B grows with interaction strength as

$$R_B \propto (C/\Delta L^6)^\gamma , \tag{6}$$

where $\gamma \approx 1/6 \pm 1\%$. This value for γ is expected since a rough estimation of the blockade radius can be made in the

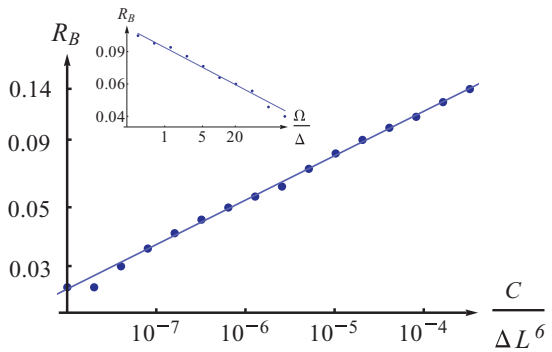

FIG. 6. (Color online) R_B as a function of C (double-log plot). The data points clearly show a power law. The parameters are $\Omega/\Delta = 0.1$ with $N = 8 = M^*$ atoms. The fit is discussed in the text. Inset: R_B as a function of Ω (double-log plot). The parameters are $C/(\Delta L^6) = 10^{-5}$ with $N = 7 = M^*$ atoms.

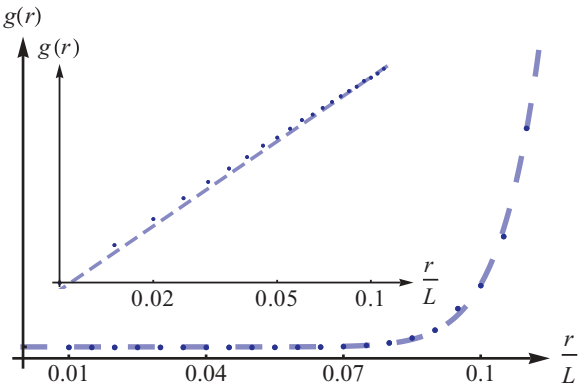

FIG. 7. (Color online) Correlation function as a function of distance. The dashed line represents a fit explained in the text. Inset: The same plot as in the main plot shown on a logarithmic scale. The parameters of the plot are $\Omega/\Delta = 1, C/(\Delta L^6) = 2 \times 10^{-5}$, with $N = 6 = M^*$ atoms.

following way [13,37,58,59]: if the blockade radius is the distance at which it becomes favorable to excite two atoms to the Rydberg state, then the interaction energy and the energy of the detuning term have to compensate. Equating these two terms leaves us with the exponent $\gamma = 1/6$. Furthermore, we find the asymptotic behavior of the correlation function for $r \ll R_B$ to be highly universal (see Fig. 7). It is given by

$$g(r) \propto r^{12}, \quad r \ll R_B. \tag{7}$$

This behavior can be understood in terms of the probability of simultaneous excitation of two neighboring atoms. Here one finds that in the regime where the interaction energy dominates over the Ω term, the probability of finding both atoms excited (in the state $|\uparrow\uparrow\rangle$),

$$P(|\uparrow\uparrow\rangle) = |\langle\uparrow\uparrow |\mathrm{GS}\rangle|^2, \tag{8}$$

is proportional to $1/V(r)^2$, where $V(r) \sim 1/r^6$ is the magnitude of the interaction contribution. In our case, this reproduces the observed behavior. Beyond the point $r = R_B$, the qualitative shape of $g(r)$ depends strongly on C see Fig. 8. While for

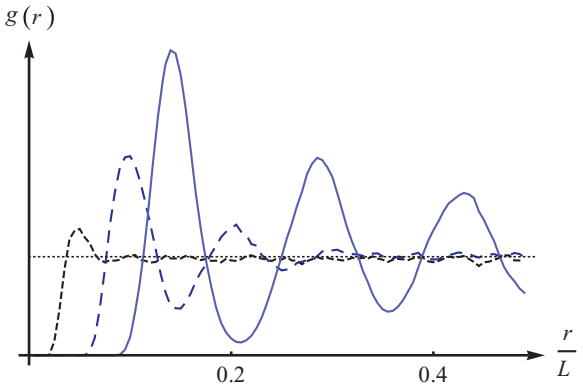

FIG. 8. (Color online) Correlation function of 1D samples measured in arbitrary units. The curves correspond to $C/\Delta L^6 = 4 \times 10^{-9}$ (dotted), $C/\Delta L^6 = 4 \times 10^{-7}$ (dashed), and $C/\Delta L^6 = 4 \times 10^{-6}$ (solid), where all other parameters remained the same: $\Omega/\Delta = 0.4$ and $N = 25$, with 300 basis states. The curves indicate that there is a critical value for $C/\Delta L^6$ between the two larger values given above.

weak interactions, $C/(\Delta L^6) < 4 \times 10^{-9}$, no additional peaks can be seen, long-range order emerges for strong interactions, $C/(\Delta L^6) > 10^{-6}$, and manifests itself as a series of equidistant peaks. In the former case, the Rydberg atoms remain in a gas phase, whereas the latter situation might by described as the Rydberg crystal proposed in Refs. [21,47]. In an ideal crystal, the additional peaks would be sharp. In our calculations, this cannot be achieved due to finite-size effects. From our simulations, we estimate the dimensionless critical parameter for the transition as $C_{\mathrm{crit}}/(\Delta L^6) \approx 5 \times 10^{-7}$ for $\Omega/\Delta \ll 1$.

This estimation can be performed in two different ways. First, we see that the "subleading" peaks gradually emerge from the noisy background with growing C. It is reasonable to assume that as soon as the peak of the highest possible order (due to the finite L) is visible, the critical C is reached. This occurs around the value for $C_{\mathrm{crit}}/\Delta L^6$ given above. Needless to say, L should be chosen to be larger than several R_B, so that a number of peaks could be observed along the whole system length.

The other method is more involved and is based upon the following criterion: we fit the correlation function data in the region $r \gtrsim R_B$ with the function

$$f(r) = 1 + \sin(ar + \phi)[Ae^{-\alpha r} + B(r/r_0)^{\beta}]. \tag{9}$$

This fitting procedure works exceptionally well for correlation functions corresponding to setups with subcritical interactions. For supercritical C, the situation changes dramatically and the fit quality rapidly deteriorates. While we cannot definitely identify the power law to dominate the large r asymptotics, its role becomes important. These radical changes in behavior of the correlation function happen at precisely the C_{crit} given above.

In fact, one can recognize this critical value for the phase transition already in the simple statistical parameter of the $P(M)$ histograms. Indeed, not only the mean value μ, but also the variance remarkably changes its behavior at approximately the same value for $C/\Delta L^6$. Both μ and σ are functions of the interaction strength C that obey power laws with certain exponents for small values of $C/\Delta L^6$ and power laws with different exponents for large $C/\Delta L^6$. The value of $C/\Delta L^6$ where the two power laws connect is the estimate of the critical value $C_{\mathrm{crit}}/\Delta L^6$, which indicates a phase transition. The behavior of μ is less prominent but still clearly detectable. Similar behavior can be seen in higher cumulants of $P(M)$. However, the larger statistical errors might make them less useful in practical applications.

IV. CONCLUSIONS

Using exact numerical diagonalization and approximative descendants of this method, we have investigated the Rydberg crystallization phenomenon in ultracold gases. We have estimated the critical interaction strength by two different techniques. Both pair-correlation function and simpler statistical data show signatures of this phase transition. The big advantage of using mean and variance of the histogram for the number of excited atoms measured in a long series of identical experiments is its good experimental accessibility. In this way, we have developed a purely statistical method

of detecting Rydberg crystallization. We hope that this procedure can soon be implemented in state-of-the-art experiments in order to unambiguously identify the Rydberg crystallization phenomenon without complicated spectroscopic techniques.

Furthermore, the presented details of the pair-correlation function might be useful for the continuous experimental efforts in spatial imaging of Rydberg aggregates in the spirit of Refs. [37,42]. This technique is not only able to yield a very precise value of the blockade radius, but has also proven to be a reliable source for the estimation of the critical parameters for Rydberg crystallization.

ACKNOWLEDGMENTS

The authors would like to thank G. Günther, M. Weidemüller, and S. Whitlock for many interesting discussions. A.K. is supported by the DFG Grant No. KO-2235/3-1, CQD and "Enable Fund" of the University of Heidelberg. T.L.S. is supported by the Swiss NSF.

[1] S. Wüster, J. Stanojevic, C. Ates, T. Pohl, P. Deuar, J. F. Corney, and J. M. Rost, Phys. Rev. A **81**, 023406 (2010).
[2] C. Ates, S. Sevincli, and T. Pohl, Phys. Rev. A **83**, 041802 (2011).
[3] C. Ates, T. Pohl, T. Pattard, and J. M. Rost, Phys. Rev. A **76**, 013413 (2007).
[4] F. Robicheaux, J. V. Hernández, T. Topçu, and L. D. Noordam, Phys. Rev. A **70**, 042703 (2004).
[5] S. Ji, C. Ates, and I. Lesanovsky, Phys. Rev. Lett. **107**, 060406 (2011).
[6] E. Urban, T. A. Johnson, T. Henage, L. Isenhower, D. D. Yavuz, T. G. Walker, and M. Saffman, Nature Phys. **5**, 110 (2009).
[7] R. Löw, H. Weimer, U. Krohn, R. Heidemann, V. Bendkowsky, B. Butscher, H. P. Büchler, and T. Pfau, Phys. Rev. A **80**, 033422 (2009).
[8] T. A. Johnson, E. Urban, T. Henage, L. Isenhower, D. D. Yavuz, T. G. Walker, and M. Saffman, Phys. Rev. Lett. **100**, 113003 (2008).
[9] T. Amthor, C. Giese, C. S. Hofmann, and M. Weidemüller, Phys. Rev. Lett. **104**, 013001 (2010).
[10] N. Samboy, J. Stanojevic, and R. Côté, Phys. Rev. A **83**, 050501 (2011).
[11] C. S. E. van Ditzhuijzen, A. F. Koenderink, J. V. Hernández, F. Robicheaux, L. D. Noordam, and H. B. van Linden van den Heuvell, Phys. Rev. Lett. **100**, 243201 (2008).
[12] A. Wetzels, A. Gürtler, L. D. Noordam, and F. Robicheaux, Phys. Rev. A **73**, 062507 (2006).
[13] R. Heidemann, U. Raitzsch, V. Bendkowsky, B. Butscher, R. Löw, L. Santos, and T. Pfau, Phys. Rev. Lett. **99**, 163601 (2007).
[14] U. Raitzsch, V. Bendkowsky, R. Heidemann, B. Butscher, R. Löw, and T. Pfau, Phys. Rev. Lett. **100**, 013002 (2008).
[15] K. P. Heeg, M. Gärttner, and J. Evers, arXiv:1202.2779.
[16] C. Ates and I. Lesanovsky, Phys. Rev. A **86**, 013408 (2012).
[17] D. Tong, S. M. Farooqi, J. Stanojevic, S. Krishnan, Y. P. Zhang, R. Côté, E. E. Eyler, and P. L. Gould, Phys. Rev. Lett. **93**, 063001 (2004).
[18] M. D. Lukin, M. Fleischhauer, R. Cote, L. M. Duan, D. Jaksch, J. I. Cirac, and P. Zoller, Phys. Rev. Lett. **87**, 037901 (2001).
[19] K. Singer, M. Reetz-Lamour, T. Amthor, L. G. Marcassa, and M. Weidemüller, Phys. Rev. Lett. **93**, 163001 (2004).
[20] I. Mourachko, D. Comparat, F. de Tomasi, A. Fioretti, P. Nosbaum, V. M. Akulin, and P. Pillet, Phys. Rev. Lett. **80**, 253 (1998).
[21] J. Schachenmayer, I. Lesanovsky, A. Micheli, and A. J. Daley, New J. Phys. **12**, 103044 (2010).
[22] H. Weimer, R. Löw, T. Pfau, and H. P. Büchler, Phys. Rev. Lett. **101**, 250601 (2008).
[23] E. Wigner, Phys. Rev. **46**, 1002 (1934).
[24] L. Jin, M. Macovei, and J. Evers, arXiv:1202.0699.
[25] C. Fabre, S. Haroche, and P. Goy, Phys. Rev. A **18**, 229 (1978).
[26] T. Amthor, M. Reetz-Lamour, S. Westermann, J. Denskat, and M. Weidemüller, Phys. Rev. Lett. **98**, 023004 (2007).
[27] W. R. Anderson, J. R. Veale, and T. F. Gallagher, Phys. Rev. Lett. **80**, 249 (1998).
[28] C. Boisseau, I. Simbotin, and R. Côté, Phys. Rev. Lett. **88**, 133004 (2002).
[29] T. J. Carroll, K. Claringbould, A. Goodsell, M. J. Lim, and M. W. Noel, Phys. Rev. Lett. **93**, 153001 (2004).
[30] T. Cubel Liebisch, A. Reinhard, P. R. Berman, and G. Raithel, Phys. Rev. Lett. **95**, 253002 (2005).
[31] A. Fioretti, D. Comparat, C. Drag, T. F. Gallagher, and P. Pillet, Phys. Rev. Lett. **82**, 1839 (1999).
[32] S. D. Hogan, P. Allmendinger, H. Saßmannshausen, H. Schmutz, and F. Merkt, Phys. Rev. Lett. **108**, 063008 (2012).
[33] M. Mudrich, N. Zahzam, T. Vogt, D. Comparat, and P. Pillet, Phys. Rev. Lett. **95**, 233002 (2005).
[34] A. L. de Oliveira, M. W. Mancini, V. S. Bagnato, and L. G. Marcassa, Phys. Rev. Lett. **90**, 143002 (2003).
[35] J. M. Raimond, G. Vitrant, and S. Haroche, J. Phys. B **14**, L655 (1981).
[36] H. Schempp, G. Günter, C. S. Hofmann, C. Giese, S. D. Saliba, B. D. DePaola, T. Amthor, M. Weidemüller, S. Sevincli, and T. Pohl, Phys. Rev. Lett. **104**, 173602 (2010).
[37] A. Schwarzkopf, R. E. Sapiro, and G. Raithel, Phys. Rev. Lett. **107**, 103001 (2011).
[38] T. Vogt, M. Viteau, A. Chotia, J. Zhao, D. Comparat, and P. Pillet, Phys. Rev. Lett. **99**, 073002 (2007).
[39] T. Vogt, M. Viteau, J. Zhao, A. Chotia, D. Comparat, and P. Pillet, Phys. Rev. Lett. **97**, 083003 (2006).
[40] A. Chotia, M. Viteau, T. Vogt, D. Comparat, and P. Pillet, New J. Phys. **10**, 045031 (2008).
[41] M. Weidemüller, Nature Phys. **5**, 91 (2009).
[42] G. Günter, M. Robert-de-Saint-Vincent, H. Schempp, C. S. Hofmann, S. Whitlock, and M. Weidemüller, Phys. Rev. Lett. **108**, 013002 (2012).
[43] This marks a difference compared to the recent publication [21], which used a lattice.
[44] F. Robicheaux and J. V. Hernández, Phys. Rev. A **72**, 063403 (2005).

[45] T. Amthor, M. Reetz-Lamour, and M. Weidemüller, *Cold Atoms and Molecules: Concepts, Experiments and Applications to Fundamental Physics* (Wiley-VCH, Berlin, 2009).
[46] We allow for interactions to act "through" the particles; that is why it is more appropriate to talk about quasi-1D systems rather than 1D ones.
[47] T. Pohl, E. Demler, and M. D. Lukin, Phys. Rev. Lett. **104**, 043002 (2010).
[48] R. M. W. van Bijnen, S. Smit, K. A. H. van Leeuwen, E. J. D. Vredenbregt, and S. J. J. M. F. Kokkelmans, J. Phys. B **44**, 184008 (2011).
[49] W. Zeller, M. Mayle, T. Bonato, G. Reinelt, and P. Schmelcher, Phys. Rev. A **85**, 063603 (2012).
[50] I. Lesanovsky, Phys. Rev. Lett. **106**, 025301 (2011).
[51] H. Weimer and H. P. Büchler, Phys. Rev. Lett. **105**, 230403 (2010).
[52] E. Sela, M. Punk, and M. Garst, Phys. Rev. B **84**, 085434 (2011).
[53] L. Mandel, Opt. Lett. **4**, 205 (1979).
[54] C. Ates, T. Pohl, T. Pattard, and J. M. Rost, J. Phys. B **39**, L233 (2006).
[55] J. V. Hernndez and F. Robicheaux, J. Phys. B **39**, 4883 (2006).
[56] M. Gärttner, K. P. Heeg, T. Gasenzer, and J. Evers, arXiv:1203.2884.
[57] W. H. Press, S. A. Teukolsky, W. T. Vetterling, and B. P. Flannery, *Numerical Recipes: The Art of Scientific Computing*, 3rd ed. (Cambridge University Press, New York, 2007).
[58] S. Sevinçli, N. Henkel, C. Ates, and T. Pohl, Phys. Rev. Lett. **107**, 153001 (2011).
[59] J. D. Pritchard, D. Maxwell, A. Gauguet, K. J. Weatherill, M. P. A. Jones, and C. S. Adams, Phys. Rev. Lett. **105**, 193603 (2010).